FULLY NONLINEAR HYPERELASTIC ANALYSIS OF NEARLY INCOMPRESSIBLE SOLIDS: ELEMENTS AND MATERIAL MODELS IN MSC/NASTRAN

by
Katerina-D. Papoulia
Senior Development Engineer
The MacNeal-Schwendler Corporation
Los Angeles, CA.

ABSTRACT

The hyperelastic elements in MSC/NASTRAN are described for 3D, plane strain and axisymmetric analysis with large strain and large rotation. The hyperelastic model used is generalized Rivlin of up to order five, extended to include the effect of compressibility at the nearly incompressible limit. Emphasis is placed on the treatment of incompressibility and the avoidance of volumetric locking. Mixed and selective reduced integration methods and the use of penalty versus Lagrange multipler techniques is discussed. Higher order elements, which effectively overcome shear locking, are presented. A series of simple and real–life examples is provided to illustrate the features of the model: extremely large strain and element distortion, volumetric and shear locking avoidance and contact applications.

1. INTRODUCTION

Version 68 of MSC/NASTRAN introduces several new elements and a new mixed formulation for the fully nonlinear analysis—in the sense of large strain and large rotation—of nearly incompressible hyperelastic materials. Although specifically developed for nearly incompressible applications (most elastomeric materials are nearly incompressible), the elements are not restricted to near incompressibility: any degree of compressibility may be admitted.

The treatment of nonlinear kinematics for these MSC/NASTRAN elements is based on classical continuum theory. The motion at each Gauss point is represented by the deformation gradient

$$\boldsymbol{F} = \frac{\partial \boldsymbol{x}}{\partial \boldsymbol{X}} = \mathbf{1} + \frac{\partial \boldsymbol{u}}{\partial \boldsymbol{X}} \tag{1}$$

where $\boldsymbol{x} = \boldsymbol{X} + \boldsymbol{u}$ is the deformed and $\boldsymbol{X}$ is the original position of the Gauss point. The formulation is total Lagrangian, in the sense that the geometry is always updated based on the original configuration. The motion may be decomposed into pure deformation (strain) and rigid body rotation through the polar decomposition theorem

$$\boldsymbol{F} = \boldsymbol{RU} = \boldsymbol{VR} \tag{2}$$

where $\boldsymbol{U} = \sqrt{\boldsymbol{F}^T\boldsymbol{F}}$ (the right stretch tensor) and $\boldsymbol{V} = \sqrt{\boldsymbol{F}\boldsymbol{F}^T}$ (the left stretch tensor) are nonlinear measures of strain and the rigid body rotation $\boldsymbol{R}$ may be (but never actually is) computed from Eq. (2). For the particular element types and material model implemented, $\boldsymbol{F}$ and $\boldsymbol{B} = \boldsymbol{F}\boldsymbol{F}^T$ are computed at each Gauss point. In this sense, the kinematics are exact and pointwise. By comparison, the large displacement/small strain corotational elements in MSC/NASTRAN use the concept of an average element rotation, thus imposing restrictions on element size. See Table 3 (Appendix A) for a comparison of the two classes of elements.

In Section 2, the element formulation is outlined, with some details given in Appendix B. In particular, the mixed displacement/pressure element interpolation for volumetric locking avoidance is discussed. In Section 3, the hyperelastic material law is presented, with emphasis on near incompressibility. Finally, some illustrative examples are given in Section 4.

2. HYPERELASTIC ELEMENTS

It has become customary to refer to the fully nonlinear elements in MSC/NASTRAN as "hyperelastic elements", although hyperelasticity is obviously not an element characteristic and does not necessarily imply a nonlinear analysis[1]. Although a hyperelastic material is not necessarily incompressible or nearly incompressible, the admittance of near incompressibility is an important characteristic of the elements' formulation. Specifically, the mixed formulation is developed to address the several problems arising in connection to near incompressibility. With a constitutive relation for the pressure in the form

1. As a matter of fact, all MSC/NASTRAN elastic material models are hyperelastic, with the exception of the isotropic elastic nonlinear model, defined on MATS1, which is empirical, based on one-dimensional data.

$$p = \sum_{i=1}^{N} 2i(J-1)^{2i-1} D_i \tag{3}$$

(see next section) it is apparent that for a very large value of some D_i $(D_i \to \infty)$ and for $J \to 1$ (J = 1 for incompressibility; see (9)), the pressure may not be determined from the constitutive relation. Numerically, this may lead to the computation of spurious stresses, ill conditioning of the stiffness matrix and volumetric locking, i.e. severe underestimation of the deformations. A cure to this situation is provided with separate (mixed) interpolations for the displacements and for the volume ratio and the pressure. This is achieved through a three field variational principle of the Hu-Washizu type [15], in which the displacements, the volume ratio and the pressure are independent variables. The corresponding energy functional is of the form

$$\Pi\left(\hat{J}, \hat{p}, \boldsymbol{u}\right) = \int_{B_0} \left[W\left(\hat{J}, \bar{I}_1, \bar{I}_2\right) + \hat{p}\left(J - \hat{J}\right) \right] dV_0 + \Pi^{ext}(\boldsymbol{u}) \tag{4}$$

where $W\left(\hat{J}, \bar{I}_1, \bar{I}_2\right)$ is the strain energy function defined in the next section. Minimization of this functional with respect to the three independent variables provides the necessary variational equations, which form the basis of the finite element implementation. Some details of the formulation are given in Appendix B. A hat, superposed on the volume ratio and on the pressure, serves to differentiate these quantities as separately interpolated independent variables from the corresponding quantities $J = \det \boldsymbol{F}$ and

$$p = \frac{\partial W}{\partial \hat{J}}\Big|_{\hat{J}=J}$$

derivable from the displacements. In a sense, $\hat{J}$ and $\hat{p}$ are averages of J and p, as indicated by (B.5), (B.6). The finite element interpolations of the three independent fields are as follows:

$$\begin{aligned} \boldsymbol{u} &= N^A(\xi)\hat{\boldsymbol{u}}_A \\ \hat{J} &= \boldsymbol{h}^T\hat{\boldsymbol{J}} \\ \hat{p} &= \boldsymbol{h}^T\hat{\boldsymbol{p}} \end{aligned} \tag{5}$$

where $N^A(\xi)$ are isoparametric shape functions and $\boldsymbol{h}$ denotes the pressure and volume ratio interpolations. The length of $\boldsymbol{h}$ is the number of "pressure nodes" available in the element. Several combinations of pressure and displacement nodes exist, as indicated in Figure 1 for plane elements. Not all of them work. The Babuska-Brezzi stability condition [3] guarantees existence, uniqueness and convergence for such elements. On a more heuristic basis, a constraint count may prove useful in assessing a mixed element: the number

$$r = \frac{\text{Total number of displacement d.o.f. in standard mesh (Fig. 1)}}{\text{total number of pressure d.o.f.}} \tag{6}$$

relating the displacement degrees of freedom (DOF) to the pressure degrees of freedom in a "standard" mesh (for discontinuous pressure elements, this is a single element mesh, as shown in Figure 1), is a good indicator of the element being under- or over-constrained [5]. This would result in spurious zero eigenvalues (spurious pressure modes) or volumetric (Poisson) locking, respectively. Optimal value of r is the one corresponding to the continuous problem, e.g., in 2D the optimal value is $r = 2/1 = 2$, i.e.

r = 2	Optimal
r > 2	Too few incompressibility constraints
r < 2	Too many incompressibility constraints
r < 1	More constraints than displacement degrees of freedom; severe locking

In Figure 1, the MSC/NASTRAN mixed formulation plane elements are indicated. In the MSC/NASTRAN elements, the pressure is either constant or linear, i.e.

$$h^T = \begin{cases} 1 & \text{for constant pressure elements} \\ (1, \xi, \eta) & \text{for linear pressure 2D elements} \\ (1, \xi, \eta, \zeta) & \text{for linear pressure solids} \end{cases} \tag{7}$$

with the number of pressure nodes being either 1 or 3 for plane elements (plane strain or axisymmetric) and either 1 or 4 for 3D solids. Generally speaking, lower order, linear displacement, elements have constant pressure interpolations and higher order, quadratic displacement, elements (with the exception of the 6-node triangle; see Figure 1) have linear pressure interpolations.

The pressure interpolations in (7) are discontinuous between elements. As a result, the fields $\hat{J}$, $\hat{p}$ may be eliminated at the element level (see Appendix B). The global problem may then be written as a standard variational problem in terms of displacements, the mixed variables $\hat{J}$, $\hat{p}$ entering the equations through some special operators of the $\overline{B}$ type, as in (B.10).

The mixed element formulation provides a general framework for the development of higher order elements. Higher order, quadratic displacement, elements were mainly developed in Version 68 of MSC/NASTRAN in order to address the problem of shear locking, i.e. the severe underestimation of element deformations in bending type problems, typical of linear displacement elements.

Whereas the relationship between selective reduced integration procedures (SRI) and mixed element formulations has been established [7], mainly for lower order elements, there are certain advantages in a mixed formulation, including its variational consistency and the generality it affords for the development of higher order elements. With selective reduced integration, the question often arises as to how the reduction of the integration order is to be performed[2] and which terms are to be selected for reduced integration. Some choices regarding the latter must be made when SRI is applied to a highly nonlinear problem, such as the large strain and large rotation applications considered here, or when volumetric-deviatoric coupling is introduced. With the mixed formulation, full Gauss point integration is performed on all integrals. The terms involving temperature strain are integrated at the nodes, using a modified Lobato scheme, in order to avoid interpolation of the temperature field.

Element stress output is in terms of Cauchy stresses (see next section) and pressure

$$\hat{p} = \frac{1}{3}(\sigma_{11} + \sigma_{22} + \sigma_{33}) \tag{8}$$

at the Gauss points (an option for nodal stress and strain output was added in Version 69). The pressure $\hat{p}$ is positive in tension.

---

2. With a lower order element this is obvious: a single point integration is performed at the center of the element.

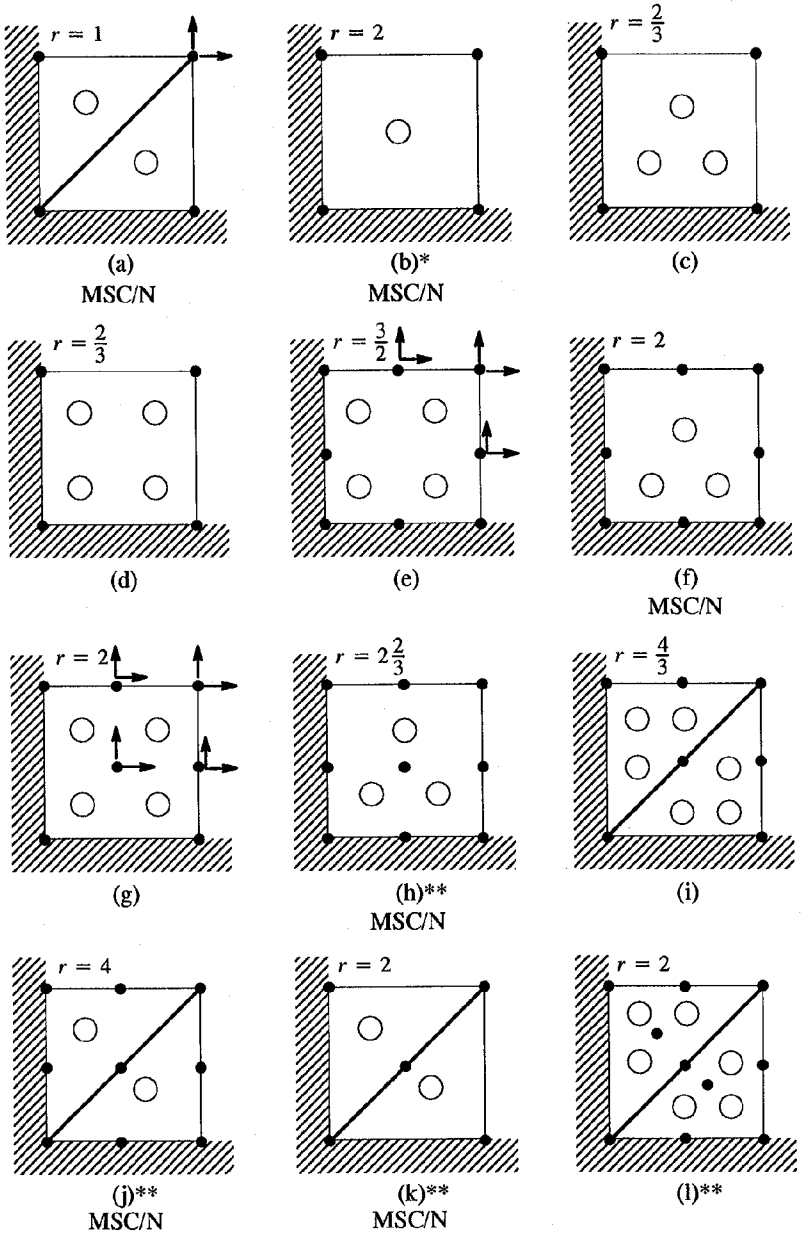

• Displacement node
◯ Pressure node

*Violates the Babuska-Brezzi condition, however exhibits optimal convergence.
**Satisfy the Babuska-Brezzi condition.

Figure 1. Discontinuous Pressure Plane Elements (After [5]).

Strain output is in terms of volumetric strain

$$\hat{J} - 1 = \frac{dV - dV_0}{dV_0} \tag{9}$$

and logarithmic strains

$$\underline{\varepsilon} = \sum_{A=1}^{3} \ln \lambda_A N_A N_A^T \tag{10}$$

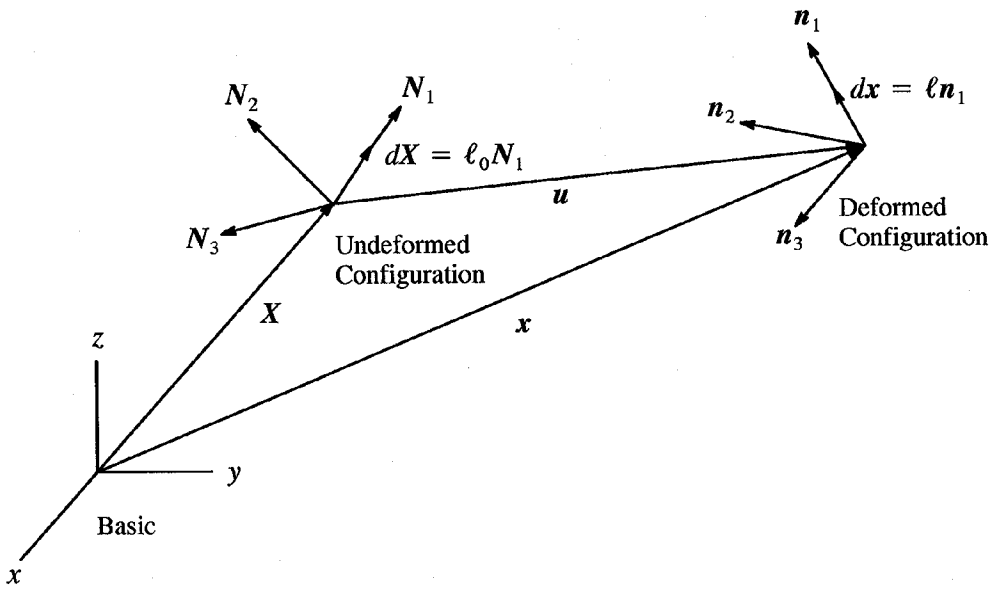

Figure 2. Principal Stretches and Rigid Body Rotations.

where λ_A, $A = 1, 2, 3$, are the principal stretches (eigenvalues of $\boldsymbol{U}$ or $\boldsymbol{V}$) and $\boldsymbol{N}_A$ are principal directions in the undeformed configuration (eigenvectors of $\boldsymbol{U}$). The nonlinear strain measure $\boldsymbol{U}$ produces length changes and relative rotation (shear strain) of all fibers, except those along the principal directions $\boldsymbol{N}_A$. This rotation is in addition to the rigid body rotation $\boldsymbol{R}$, which rotates all fibers by the same amount. A vector $d\boldsymbol{X}$ of length ℓ_0 which, in the undeformed configuration, is along one of the directions $\boldsymbol{N}_A$, will undergo a stretch and a rigid body (only) rotation (Figure 2). After deformation, the vector $d\boldsymbol{x} = \boldsymbol{F}d\boldsymbol{X}$, of length ℓ, will be positioned along the direction $\boldsymbol{n}_A = \boldsymbol{R}\boldsymbol{N}_A$, which is an eigenvector of $\boldsymbol{V}$. The principal stretch λ_A provides a measure of the deformation (stretch)

$$\lambda_A = \frac{\ell}{\ell_0}. \tag{11}$$

The physical meaning of the logarithmic strain tensor is debatable in all but the principal directions. In principal directions, the logarithmic strain may be seen as that producing an infinitesimal change per unit current length

$$d\varepsilon_A = \frac{d\ell}{\ell}$$
$$\varepsilon_A = \ln\frac{\ell}{\ell_0} \quad . \tag{12}$$

Whereas for logarithmic strain rates this meaning is retained in the general three dimensional case (i.e., the logarithmic strain rate is the rate at which stretching occurs), the logarithmic strains themselves are integrated quantities, with no specific physical meaning [8].

In the case of temperature, total strains, including both the mechanical and temperature parts, are recovered. All output is in the basic coordinate system. For plane strain elements an option is provided for a user specified coordinate system [9].

3. HYPERELASTIC (GREEN ELASTIC) MATERIAL

A Green elastic material is one for which a function W of the strains exists[3], called the strain energy function, such that

$$\boldsymbol{S} = \frac{\partial W}{\partial \boldsymbol{E}} \tag{13}$$

where $\boldsymbol{E} = (\boldsymbol{U}^2 - \mathbf{1})/2$ is a measure of strain (Green-Lagrange) and $\boldsymbol{S}$ is the second Piola-Kirchhoff stress, a symmetric referential stress defined as

$$\boldsymbol{SN} = \frac{\boldsymbol{F}^{-1}d(\text{force})}{d(\text{undeformed area})} \tag{14}$$

where $\boldsymbol{N}$ is the normal to the undeformed area at the point, where the stress is computed. A physically more meaningful quantity is the Cauchy (for that reason also called "true") stress $\underline{\sigma}$, defined such that

$$\underline{\sigma}\boldsymbol{n} = \frac{d(\text{force})}{d(\text{deformed area})} \tag{15}$$

where $\boldsymbol{n}$ is the normal to the deformed area at the point, related to the Piola stress as follows:

$$\underline{\sigma} = \frac{1}{J}\boldsymbol{F}\boldsymbol{S}\boldsymbol{F}^T. \tag{16}$$

The generalized Rivlin model, available in MSC/NASTRAN, possesses a strain energy function of the form

$$W\left(\hat{J}, \bar{I}_1, \bar{I}_2, T\right) = \sum_{i,j\geq 0}^{N_A} A_{ij}\left(\bar{I}_1 - 3\right)^i\left(\bar{I}_2 - 3\right)^j + \sum_{i=1}^{N_D} D_i\left(\hat{J} - 1 - \alpha_v(T - T_0)\right)^{2i} \tag{17}$$

---

3. Based on considerations of invariance of the constitutive law under superposed rigid body motion, W may not be a function of the rigid body rotation $\boldsymbol{R}$.

with $A_{00} = 0$. This is an uncoupled relationship between the volumetric part of the deformation, represented by $\hat{J}$ and the distortional part, represented by the invariants

$$\bar{I}_1 = \mathrm{tr}\overline{\boldsymbol{B}} \tag{18}$$

$$\bar{I}_2 = \frac{1}{2}\left[(\mathrm{tr}\overline{\boldsymbol{B}})^2 - \overline{\boldsymbol{B}} : \overline{\boldsymbol{B}}\right]$$

where $\overline{\boldsymbol{B}} = J^{-2/3}\boldsymbol{B} = \overline{\boldsymbol{F}}\overline{\boldsymbol{F}}^T$; $\overline{\boldsymbol{F}} = J^{-1/3}\boldsymbol{F}$ represents the volume preserving (distortional) part of the deformation [12], tr is the trace operator ($\mathrm{tr}\overline{\boldsymbol{B}} = \overline{B}_{11} + \overline{B}_{22} + \overline{B}_{33}$) and : stands for double contaction (i.e. $\overline{\boldsymbol{B}} : \overline{\boldsymbol{B}} = B_{ij}\,B_{ij} = \overline{B}_{11}^2 + \overline{B}_{22}^2 + \overline{B}_{33}^2 + 2\overline{B}_{12}^2 + 2\overline{B}_{23}^2 + 2\overline{B}_{13}^2$). With the use of strain invariants, the model is implicitly isotropic. An anisotropic hyperelastic model has not been implemented for large strains.

The effect of temperature is included in the volumetric part of the deformation. Note that α_V is the volumetric coefficient of thermal expansion, $\alpha_V = 3\alpha$ for an isotropic material; T is the current and T_0 is the initial temperature. The coefficients A_{ij} (up to 20, corresponding to $N_A = 5$) and D_i (up to 5 coefficients, corresponding $N_D = 5$) may be either provided by direct input or determined from experimental data provided by the user [12]. A_{ij} and D_i may not be temperature dependent.

Application of (13), (16) and use of the chain rule results in the following stress-strain relationship:

$$\underline{\sigma} = \hat{p}\mathbf{1} + \frac{2}{J}\mathrm{dev}\left[\left(\frac{\partial W}{\partial \bar{I}_1} + \bar{I}_1\frac{\partial W}{\partial \bar{I}_2}\right)\overline{\boldsymbol{B}} - \frac{\partial W}{\partial \bar{I}_2}\overline{\boldsymbol{B}}\overline{\boldsymbol{B}}\right], \tag{19}$$

where dev denotes the deviatoric part of a matrix, $\mathrm{dev}(\cdot) = (\cdot) - (1/3)\,\mathrm{tr}(\cdot)\,\mathbf{1}$, and $\hat{p}$ is the independently interpolated pressure. Note the use of J and $\hat{J}$ in the above and in the variational equations in Appendix B.

A hyperelastic material is not necessarily incompressible or nearly incompressible. However, the form (17) of the strain energy function, in terms of distortional and dilatational components, is chosen in anticipation of nearly incompressible applications. Only then is the additional mathematical complexity, introduced by the decomposition of the motion into a volume preserving distortional and a dilatational part, justified by the separate treatment of these components, either through the mixed formulation or through SRI. It should be noted that the model, with the first term of (17) only, was originally developed by Rivlin [14] for an incompressible material. Equation (17) represents, in fact, an appropriate extension to include compressibility at the nearly incompressible limit, in which D_i, when large, may be regarded as penalty values for imposing the incompressibility constraint.

The degree of compressibility is controlled by the value of the dilatational (volumetric) coefficients D_i relative to the value of the distortional coefficients A_{ij}. In the limit of small strains, these are related to the familiar quantities K (the bulk modulus) and G (the shear modulus) as follows:

$$K = 2D_1 \tag{20}$$

$$G = 2(A_{10} + A_{01})\,.$$

As incompressibility increases, numerical problems arise. Our experience is that the mixed formulation will safely address these problems up to $K/G = 1000$, or $D_1 = (A_{10} + A_{01}) \times 10^3$ (the default for D_1 in MSC/NASTRAN). At small strains, this corresponds to a Poisson's ratio of 0.4995. It is a conservative estimate: higher values of the bulk modulus may be admitted in certain situations. In general, problems are likely to occur at very high compressive pressures, of the order of the bulk modulus, in nearly incompressible applications. Such pressures typically arise in highly constrained parts under compression. The effect usually is an ill-conditioned stiffness matrix, due to an apparent material instability.

For the above reasons and to address higher levels of incompressibility (i.e. materials with $0.4995 \leq \nu \leq 0.5$), some codes choose to impose the incompressibility constraint explicitly, through a Lagrange multiplier technique [1] (full incompressibility). Whereas this may have numerical advantages, caution must be exercised, as the incompressibility assumption may lead to errors, as, for example, in the case of very thin bonded layers of nearly incompressible material under compression, where severe overestimation of the compressive stiffness due to the assumption of incompressibility has been observed [13]. The new mixed formulation of MSC/NASTRAN has been capable of solving several problems of this type. In particular, a fully constrained cube, of a material with $G = 1.25$ MPa and $K = 1500$ MPa, has been successfully compressed to 20% of its original length, developing a pressure of $p = 1340$ MPa. In such situations, the full Newton method (ITER,1 on the NLPARM entry) usually works better than the automatic updating of the stiffness (AUTO).

4. EXAMPLES

A set of examples has been chosen, which illustrate the effect of shear locking and its successful avoidance using higher order elements; volumetric locking avoidance for all elements; element performance (mixed versus SRI) and the use of the new triangular and axisymmetric elements; the interaction of hyperelastic elements with other MSC/NASTRAN nonlinear capabilities, namely geometric nonlinearity and contact; and a large scale computation involving highly dissimilar materials under severe conditions of combined compression and shear.

4.1 Volumetric and Shear Locking Tests

These are simple tests to evaluate the elements against volumetric (Poisson's ratio) and shear locking and are both taken from the MacNeal-Harder proposed standard test library [6]. The volumetric locking tests are performed on a thick walled cylinder of inner radius 3.0 in, outer radius 9.0 in and thicknes of 1.0 in, loaded by a unit pressure at the inner radius. The material properties are $E = 10^3$ psi and $\nu = 0.49$, 0.499 and 0.4999 successively. The problem is solved with plane strain, axisymmetric and solid elements, with appropriate axisymmetric boundary conditions and the results compared to an analytical solution. Due to the mixed formulation, all elements almost perfectly match the analytical solution (to within 0.7%). Some locking is observed in the TRIA3 element (a 14% underestimation of the displacement at the inner radius for $\nu = 0.4999$).

The shear locking tests consist of a cantilever beam, modeled with regular, trapezoidal and parallelogram elements, subjected to a unit force at the free end in the vertical direction (Figure 3).

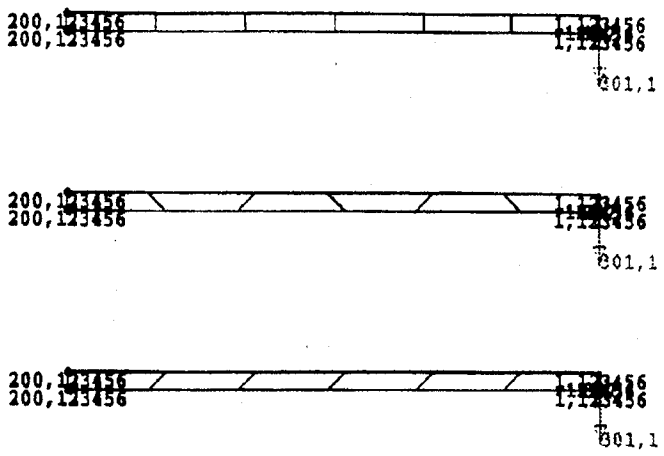

Figure 3. Shear Locking Tests.

The problem is solved with plane strain and solid elements (a Poisson's ratio $\nu = 0$ is selected to make the two solutions equivalent). As expected, all lower order elements fail this test, due to shear locking (no provision against shear locking is made in the lower order elements). As a result of their quadratic displacement interpolations, the higher order hexahedral and quadrilateral elements match the analytical solution and effectively solve the shear locking problem. The higher order triangular, pentahedral and tetrahedral elements, while providing satisfactory results with the regular mesh, still exhibit locking with the trapezoidal and parallelogram meshes. The following example is another illustration of the effect of shear locking.

4.2 Rubber Bushing Problem

A bushing, consisting of a rubber part, perfectly bonded to a rigid frame and internal shaft, is subjected to a vertical load, applied to the top grid point of the inner wall (Figure 4). The goal of the analysis is to demonstrate the ability of higher order elements to overcome the shear locking, reported for the same problem in [12]. The analysis is performed with plane strain and solid linear and quadratic elements. Considering symmetric conditions, one-half of the rubber part is modeled (Figure 5). The grid points on the outer boundary are fully constrained to simulate the rubber-frame interface, while, on the inner boundary, the horizontal degrees of freedom are constrained and the vertical degrees of freedom are tied together with MPC's. Rubber is modeled as a hyperelastic material with $A_{10} = 0.177$ N/mm^2, $A_{01} = 0.045$ N/mm^2, and $D_1 = 333$ N/mm^2. As demonstrated by the force-displacement curve of Figure 4, the finite element solution using linear displacement, lower order quadrilaterals is acceptable only up to a load $P \cong 200$ N.

For higher values of the load, shear locking takes over and the solution becomes overly stiff. With the higher order elements, however, an acceptable solution is obtained, which tends to the exact [16]. The same behavior may be examined on the deformed meshes of Figure 5. For the same level of load, the 9-noded quadrilaterals exhibit a level of deformation, much higher than that of the linear displacement, 4-noded ones, which lock. Similar behavior is obtained with the higher order triangular, pentahedral and tetrahedral elements, all of which successfully solve this problem and avoid shear locking, while their lower order counterparts do not. In particular, the locking exhibited by the 3-noded triangle is so severe, that practically no deformation is

obtained

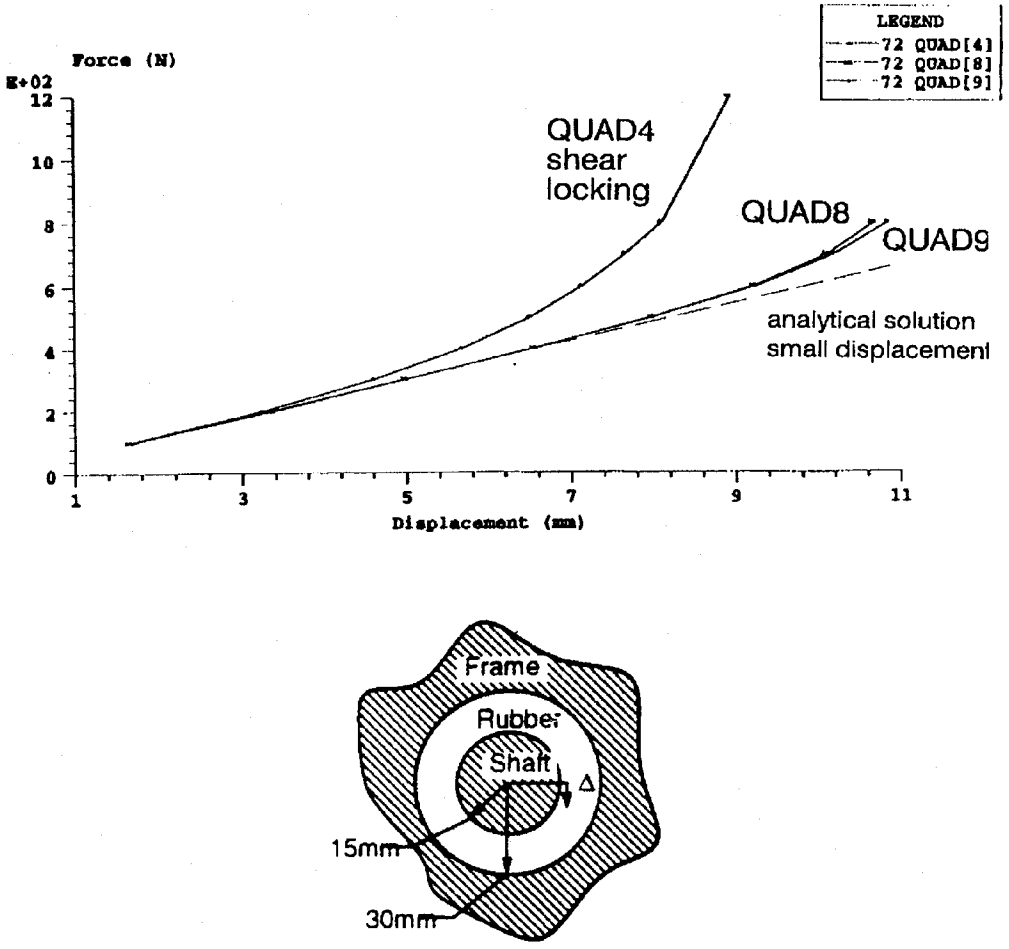

Figure 4. Rubber Bushing Problem.

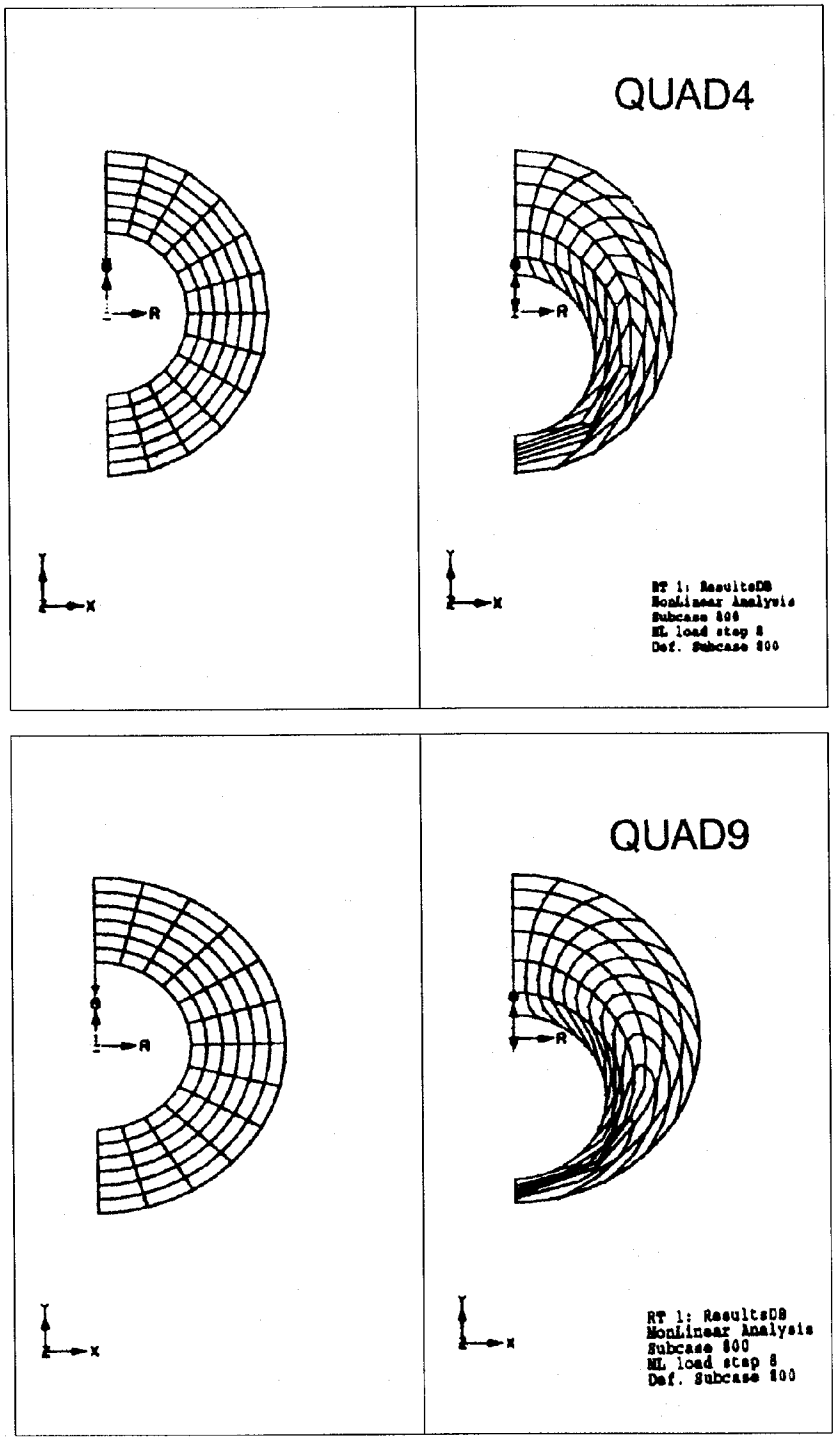

Figure 5. Rubber Bushing Problem: Finite Element Meshes and Deformed Shapes.

4.3 Lateral Compression of a Rubber Cylinder

This classical example combines the hyperelastic with the contact capability. An infinitely long cylinder with a diameter of 0.4 m is compressed between two rigid plates. The material is rubber with $A_{10} = 0.293$ N/mm^2, $A_{01} = 0.177$ N/mm^2 and $D_1 = 705$ N/mm^2 [16]. The problem was presented in [12] using quadrilateral elements. It is repeated here, with the load increased to 4.0 N, to illustrate the performance and use, as fillers, of the new triangular elements.

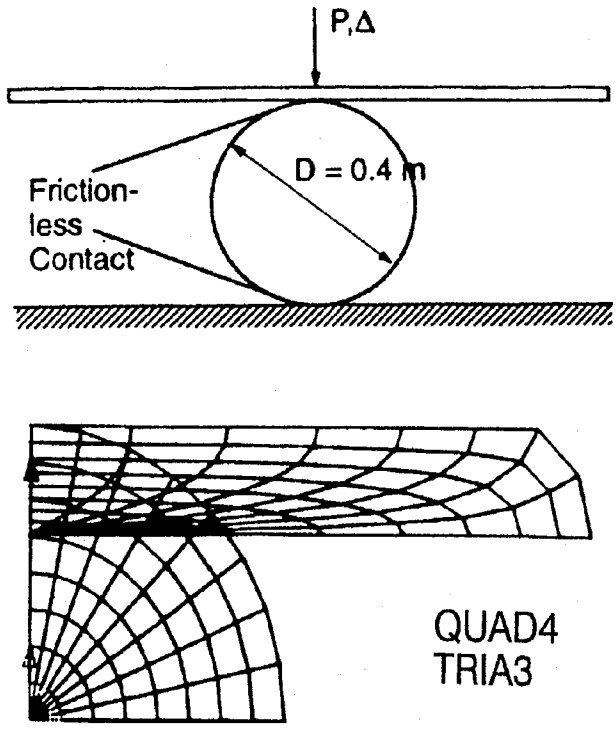

Figure 6. Compression of Rubber Cylinder.

4.4 Pressure of a Circular Plate

A circular plate 15 inches in diameter and 0.5 in thick is simply supported along the edge and is subjected to a uniform pressure [10]. The material is hyperelastic with $A_{10} = 80$ psi, $A_{01} = 20$ psi and $D_1 = 50,000$ psi. The problem is solved using solid and axisymmetric elements. The solid model represents a 10° segment, with appropriate axisymmetric boundary conditions. The pressure is applied as a follower force (PLOAD4 and PLOADX1) in 7 subcases, corresponding to 3, 15, 25, 30, 35, 40, and 45 psi.

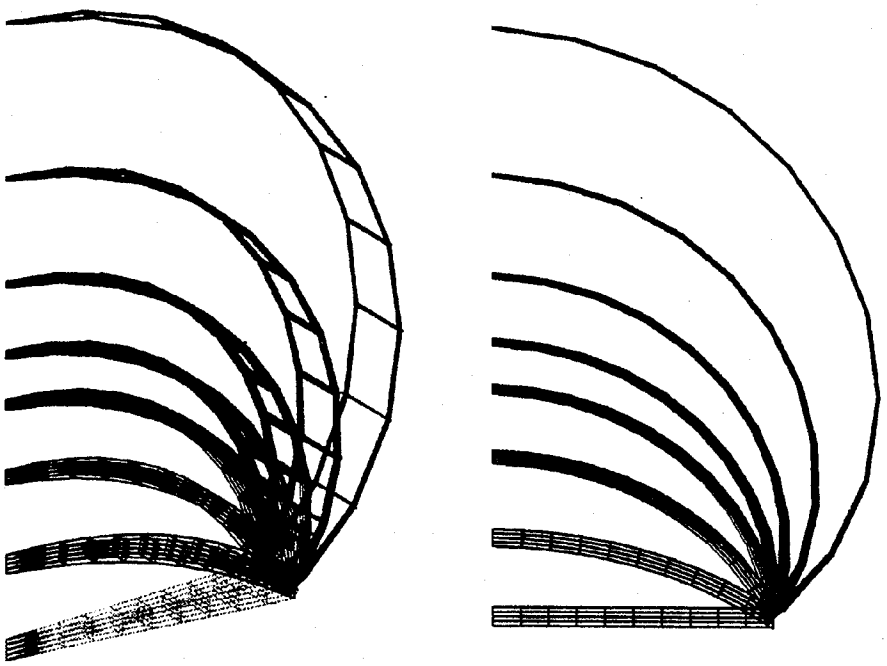

Figure 7. Pressure of a Circular Plate: Solid and Axisymmetric Elements.

Table 1 shows, for each subcase, the maximum (over load steps) number of iterations for convergence. A comparison is made, for solid elements, between the mixed formulation of Version 68 and the selective reduced integration method, available in Version 67.5 of MSC/NASTRAN. Axisymmetric elements (only available in Version 68) are also included. The first number in each cell is the maximum number of iterations using the full Newton (ITER,1) method, whereas the second is the maximum number of iterations with AUTO. It is seen that the mixed formulation reduces the number of iterations and successfully increases the pressure to 45 psi. The large number of iterations at high pressures is due to the fact that the effect of follower force has not been included in the element stiffness. To illustrate this point, the axisymmetric case with a non-follower pressure, showing a significantly reduced number of iterations at high pressures, is included in the Table (ITER,1 calculations).

Table 1. Maximum Number of Iterations for Circular Plate Under Pressure.

	Subcase 3	Subcase 15	Subcase 25	Subcase 30	Subcase 35	Subcase 40	Subcase 45
Mixed	15 44	7 14	9 10	10 13	15 18	25 19	37 18
SRI	20 35	16 16	28 16	40 17	99 25	– 39	– 64
Axisymmetric Mixed	20 42	22 23	24 23	25 19	36 30	49 35	70 37

	Subcase 3	Subcase 15	Subcase 25	Subcase 30	Subcase 35	Subcase 40	Subcase 45
Axisymmetric No Follower Force	21	23	14	9	9	10	10

4.5 Compression/Shear of a Vibration Isolator

Vibration isolators consist of alternate layers of elastomer and steel, designed as to provide effecctive isolation in the horizontal, mostly, direction, due to their low shear stiffness, while supporting high vertical loads. Due to the very dissimilar nature of the two materials and to the highly constrained conditions in the rubber layers, as well as to the very high strains involved and the size of the problem, they present serious difficulties in their numerical solution. A low shape factor isolator (relatively thick rubber layers) is solved here, for which experimental results are available [2]. The model consists of 2592 eight-noded hexahedral elements for the rubber and 192 four-noded quadrilateral shell elements, with geometric nonlinearity included, for the reinforcing plates. Contact surfaces are specified between the vertical faces and the bottom and top plates, which are considered rigid. Due to symmetry, half the isolator is analyzed (Figure 8). A total vertical load of 31,800 lbs is applied (corresponding to an applied pressure of ~ 500 psi) and kept constant during the analysis. Following application of the vertical load, a horizontal force of 37,500 lbs is applied in 200 load increments (half the loads are applied to the finite element mesh). The rubber is modeled as a hyperelastic material with $A_{10} = 80$ psi and D_1 the default value of $1000A_{10}$, to simulate near incompressibility. The steel plates, whose thickness is 0.105 in, are assumed linear elastic with $E = 30 \times 10^6$ psi and $\nu = 0.3$. Figure 8 shows the compressed isolator in a 3D view and the deformed shape at 37,500 lbs horizontal load (500% shear strain). A comparison with the experiment and with results obtained with MARC [4] is given in Table 2. The simple choice of material model accounts for the relative linearity of the results. The horizontal load of 18,750 lbs is the last reported converged step with MARC [4]. In the present analysis the load was increased to 37,500 lbs with no convergence difficulties.

Table 2. Maximum Displacements of Vibration Isolator.

	31,800 lbs Compression			31,800 lbs Compression 18,750 lbs Shear			31,800 lbs Compression 37,500 lbs Shear		
	MSC/N	MARC	Test	MSC/N	MARC	Test	MSC/N	MARC	Test
Vertical disp.	0.259	0.241	0.254	0.547	–	–	1.214	–	–
Horizontal disp.	–	–	–	6.89	6.92	6.40	13.44	–	–

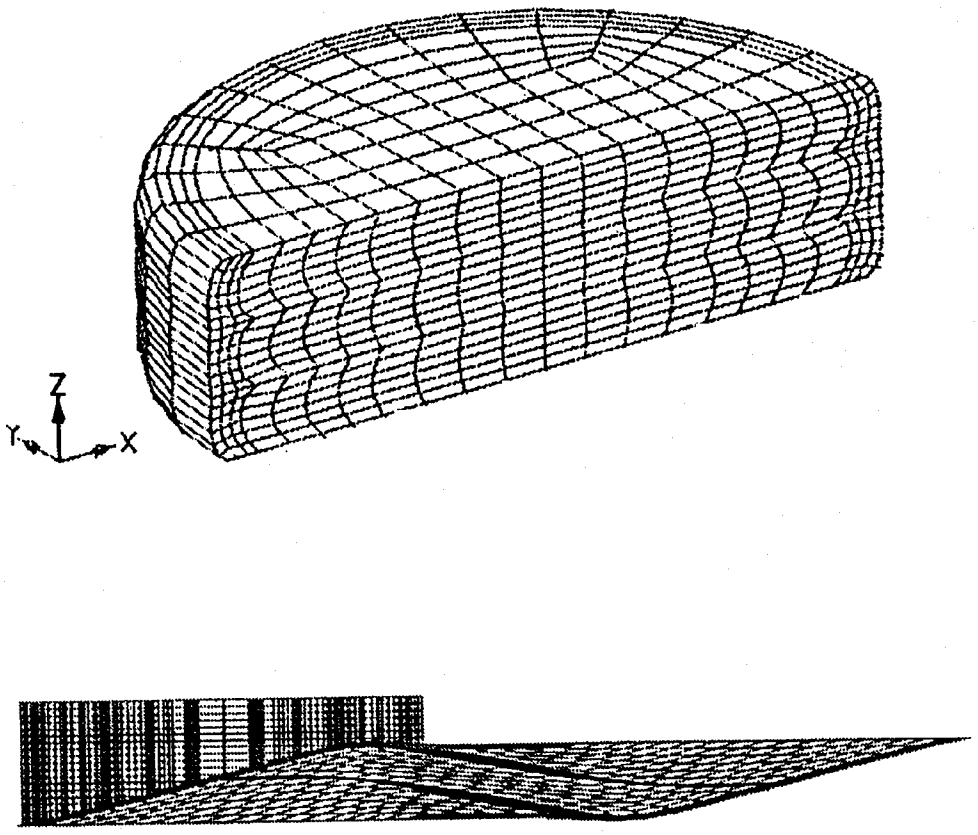

Figure 8. Compression and Compression/Shear of Multilayered Vibration Isolator.

5. CONCLUSIONS

A mixed formulation for nearly incompressible hyperelasticity at finite strains, implemented in Version 68 of MSC/NASTRAN, has been presented. Comparison has been made with selective reduced integration procedures in MSC/NASTRAN Version 67.5. The effective use of higher order elements in avoiding shear locking in bending type applications has been demonstrated.

ACKNOWLEDGMENTS

The knowledgable contributions of Dr. Bhoomaiah Alishetti of MSC in coding the hyperelastic elements into Version 68 of MSC/NASTRAN are greatly appreciated. By constructing a DMAP[4] alter, which numerically evaluates the stiffness, Bob Harder, Chief Scientist of MSC, was able to show that the hyperelastic element tangent is consistent with the element internal force vector to within 0.01%. The ingenuity of his effort, as

4. DMAP is MSC/NASTRAN's macro-level language.

well as his enthusiasm, are gratefully acknowledged.

REFERENCES

[1] *ABAQUS Users Manual.*

[2] Aiken, I.D., Kelly, J.M. and Tajirian, F.F., "Mechanics of Low Shape Factor Elastomeric Seismic Isolators", Report No. UCB/EERC–89/13, University of California, Berkeley.

[3] Babuska, I., "The Finite Element Method with Lagrangr Multipliers", Num. Math., 20, 179–192, 1973.

[4] Billings, L.J. and Shepherd, R., "The Modeling of Layered Steel/Elastomer Seismic Base Isolation Bearings", MARC 1992 Users Conference, Monterey, CA, September 3–4, 1992.

[5] Hughes, T.J.R., *The Finite Element Method*, Prentice Hall, 1987.

[6] MacNeal, R.H. and Harder, R.L, "A Proposed Standard Set of Problems to Test Finite Element Accuracy", *Finite Elements in Analysis and Design*, 1, 3–20, 1985.

[7] Malkus, D.S. and Hughes, T.J.R., "Mixed Finite Element Methods-Reduced and Selective Integration Techniques: A Unification of Concepts", CMAME, 15, 63–81, 1978.

[8] Malvern, L., *An Introduction to the Mechanics of Continuous Media*, Prentice-Hall, 1969.

[9] *MSC/NASTRAN Release Notes* for Version 68.

[10] Oden, J.T., *Finite Elements of Nonlinear Continua*, McGraw-Hill, 1972.

[11] Papoulia, K.D., "Software Requirement Specification for New Hyperelastic Elements", The MacNeal-Schwendler Corporation, KDP–05, March 1993.

[12] Papoulia, K.D. and Hsieh, S.S., "Large Deformation Hyperelastic Analysis in MSC/NASTRAN Version 67.5", Proceedings, MSC/NASTRAN World Users Conference, Arlington, VA, May 1993.

[13] Papoulia, K.D. and Kelly, J.M., "The Compression of Bonded Blocks of Soft Elastic Material: A Variational Solution", *ASCE J. Engng Mechs,* to appear.

[14] Rivlin, R.S., "A Note on the Torsion of an Incompressible Highly Elastic Cylinder", Proc. Cambridge Phil. Society, 45, 485–487, 1949.

[15] Simo, J.C. and Taylor, R.L., "Quasi-Incompressible Finite Elasticity in Principal Stretches. Continuum Basis and Numerical Algorithms", *CMAME, 85, 273–310, 1991.*

[16] Sussman, T. and Bathe, K.–J., "A Finite Element Formulation for Nearly Incompressible Elastic and Inelastic Analysis", *Computers and Structures, 26, 1/2, 357–409, 1987.*

APPENDIX A: NONLINEAR ELEMENTS IN MSC/NASTRAN

The following table provides a list of available elements and their associated property and material characteristics, as well as a comparison between the fully nonlinear and geometric nonlinear elements. In Versionn 68, a complete family of plane strain, axisymmetric and solid elements is provided for fully nonlinear hyperelastic analysis (see [9] for more details).

Table 3. Nonlinear Elements in MSC/NASTRAN.

Element	Fully Nonlinear (Finite Deformation) Analysis		Geometrically Nonlinear Analysis	
	Large Strain + Large Rotation		Large Rotation	
	Total Lagrangian Formulation Pointwise Element Rotation Nonlinear Strain Measure		Corotational Formulation Average Elementt Rotation Linear Strain Measure	
	Activated by Property Entry		Activated by PARAM,LGDISP,1	
	Plane Strain	Membrane/ Bending	Plane Strain	Membrane/ Bending
CQUAD4 CQUAD8 CQUAD CTRIA3 CTRIA6	PLPLANE MATHP	–	PSHELL with MID=-1 MAT1, MATS1 e.t.c. Lower Order Elements Only	PSHELL MAT1, MATS1 e.t.c. Lower Order Elements Only
CQUADX CTRIAX	Axisymmetric PLPLANE, MATHP		–	
CHEXA CPENTA CTETRA	PLSOLID MATHP		PSOLID MAT1, MATS1 e.t.c. Lower Order Elements Only	

APPENDIX B: SUMMARY OF MIXED FORMULATION

Some details of the fully nonlinear mixed finite element formulation [11] are provided: Minimization of the Hu-Washizu functional (4), with respect to the displacements, leads to the virtual work equation

$$\delta\Pi^{int} + \delta\Pi^{ext} = 0 \tag{B.1}$$

$$\delta\Pi^{int} = \int_{B_0} \boldsymbol{S}^T \delta\boldsymbol{E} dV_0 = \int_{B} \underline{\sigma}^T \nabla^s(\delta\boldsymbol{u}) dV \tag{B.2}$$

whereas minimization with respect to the mixed variables $\hat{J}, \hat{p}$ leads to the additional equations

$$\int_{B_0} \delta\hat{J}\left(\frac{\partial W}{\partial \hat{J}} - \hat{p}\right) dV_0 = 0 \tag{B.3}$$

$$\int_{B_0} \delta\hat{p}\left(J - \hat{J}\right) dV_0 = 0 \tag{B.4}$$

Upon introducing the finite element interpolations (5) into (B.3), (B.4), closed form expressions at the element level may be obtained [15]:

$$\hat{J} = \boldsymbol{h}^T \boldsymbol{H}^{-1} \int_{B_0} \boldsymbol{h} J dV_0 \tag{B.5}$$

$$\hat{p} = \boldsymbol{h}^T \boldsymbol{H}^{-1} \int_{B_0} \boldsymbol{h} \frac{\partial W}{\partial \hat{J}} dV_0 \tag{B.6}$$

where

$$\boldsymbol{H} = \int_{B_0} \boldsymbol{h}\boldsymbol{h}^T dV_0 \ . \tag{B.7}$$

The stiffness matrix is obtained through linearization of the internal virtual work at the undeformed geometry:

$$\delta\Pi^{int} = \int_B \underline{\sigma}^T \nabla^s(\delta \boldsymbol{u}) dV = \int_{B_0} J\sigma : \frac{\partial(\delta \boldsymbol{u})}{\partial \boldsymbol{X}} \boldsymbol{F}^{-1} dV_0 \tag{B.8}$$

i.e.

$$\Delta\left(\delta\Pi^{int}\right) = \int_{B_0} \left[\Delta(J\sigma) : \nabla(\delta \boldsymbol{u}) + J\sigma : \mathrm{GRAD}(\delta \boldsymbol{u}) \Delta \boldsymbol{F}^{-1}\right] dV_0 \tag{B.9}$$

The final result is

$$\Delta(\delta\Pi^{int}) = \int_B \Big(\hat{p}\ \mathrm{tr}\nabla(\Delta\boldsymbol{u})\mathrm{tr}\nabla(\delta\boldsymbol{u}) + \mathrm{dev}\nabla^s(\Delta\boldsymbol{u}) : \mathbf{C}^S : \mathrm{dev}\nabla(\delta\boldsymbol{u}) + \nabla(\Delta\boldsymbol{u})\underline{\sigma} : \nabla(\delta\boldsymbol{u}) - 2\nabla^s(\Delta\boldsymbol{u})\underline{\sigma} : \nabla^s(\delta\boldsymbol{u}) \Big) dV + \overline{\boldsymbol{B}}^T[\delta\boldsymbol{u}] \int_{B_0} \frac{\partial W}{\partial \hat{J}^2} \boldsymbol{h}\boldsymbol{h}^T dV_0\ \overline{\boldsymbol{B}}[\Delta\boldsymbol{u}] \tag{B.10}$$

where $\mathbf{C}^S$ is a material constitutive tangent and the operator $\overline{\boldsymbol{B}}[\ \cdot\ ]$ is defined as

$$\overline{\boldsymbol{B}}[\cdot] \equiv \boldsymbol{H}^{-1} \int_B \boldsymbol{h}\mathrm{tr}\nabla(\cdot)dV \tag{B.11}$$

with the matrix $\boldsymbol{H}$ defined in Eq. (B.7). Note that all integrals and shape function derivatives are evaluated in the current (deformed) geometry.